Geochemical Perspectives Letters

© 2024 The Authors
Published by the European Association of Geochemistry

Neoarchean marine chemical sediments as archives of Hadean silicate differentiation

A.N. Wainwright, V. Debaille, J.E. Hoffmann, S. Viehmann, M. Bau

Supplementary Information

The Supplementary Information includes:

- Regional geology and sample description
- Methods
- Trace Elements
- $^{143}Nd/^{144}Nd$ modelling
- Tables S-1 to S-3
- Figures S-1 to S-5
- Supplementary Information References

Regional geology and sample description

The Temagami BIF is part of the Temagami Greenstone Belt that is located in the Neoarchean Abitibi Greenstone succession, Ontario, Canada. The up to 200 m thick Algoma-type BIF is associated with (meta)sedimentary and (meta)volcanic units (Fig. S-1). The here studied BIF samples originate from a road cut on Highway 11 north of the village of Temagami (47°04‘24’’ N; 79°47’31’’ W). The BIF consist of alternating chert and magnetite mesobands (Fig. S-2) and experienced only lower greenschist facies metamorphism (Fyon and Cole, 1989). Both magnetite and chert bands show no geochemical evidence for detrital aluminosilicate contamination (Bau and Alexander, 2009; Viehmann *et al.,* 2014; Bau *et al.,* 2022; Mundl-Petermeier *et al.,* 2022). The depositional age of the BIF is bracketed by U-Pb zircon ages of 2736 ± 3 Ma from underlying metavolcanics and 2687 ± 2 Ma of a crosscutting rhyolitic dyke (Bowins and Heaman, 1991). Individual chert and magnetite bands of the BIF were recently directly dated via the radiogenic Sm-Nd and Lu-Hf isotopes and yield 2605 ± 140 Ma and 2760 ± 120 Ma, respectively, overlapping with the proposed depositional age and suggesting negligible impact of post-depositional overprints (Viehmann *et al.,* 2014).

Methods

In sections TM1 and TM2 two adjacent layers were analysed, while in section TM3 five adjacent layers (3 chert and 2 magnetite) were analysed. Due to the large amount of sample powder required for these analyses, all samples were re-sampled from previous studies (Bau and Alexander, 2009; Viehmann *et al.,* 2014), but are similar to those used in

Mundl-Petermeier *et al*. (2022). Individual chert and magnetite were separated by a diamond saw and then homogenised in an agate mill. This technique could have resulted in less pristine separation relative to micro-drill samples, for example for samples TM 3-3 and TM3-4 that are suspected to have been mixed, possibly due to the faulting in the sample (see Fig. S-3).

Approximately 1 g of each sample were weighed and digested using a mixture of concentrated HNO_3 and HF followed by HCl in closed Savillex beakers. After digestion a 5% aliquot was taken for isotope dilution analysis of Nd and Sm. The remaining solution was processed for unspiked Nd compositions; the separation procedure used was adapted from Debaille *et al.* (2013). In brief, five separate columns are used to purify Nd from Ce and Sm. Firstly, Fe is removed with anion resin, then the Nd was purified from the matrix first with ~2 ml of AG50W-X8 cation resin (200-400 mesh). The matrix was eluted in 2N HCl and the REE cut was collected in 6N HCl. This was subsequently purified by HDEHP (di-2ethylhexyl-orthophosphoric acid)-coated Teflon powder where a Nd cut was obtained containing traces of Ce. For ensuring efficient removal of Ce from the Nd cut due to the isobaric interference on mass 142, a second HDEP column was used following the procedure of Li *et al.* (2015). In brief, Ce is oxidised as Ce^{4+} using NaBrO3 in HNO3 and as such sticks on the HDEHP resin, while Nd in 3+ state is eluted. The final column used 0.5 ml of AG50X8 resin, to remove the Na added during the Ce clean-up column, recovering Nd in 6N HCl. The total recovery of Nd was better than 99%, hence avoiding any potential nuclear field shift effect (Saji *et al.,* 2016). Total procedural blanks are 72 ppt of Nd and 15 ppt of Sm.

The isotope dilution aliquots are spiked with a ^{150}Sm-^{148}Nd mixed spike. Neodymium and Sm were purified from the matrix using a two-column ion-exchange technique as detailed in Debaille *et al.* (2013). First, a column composed of ~2 ml of AG50W-X8 cation resin (200-400 mesh) separates the REE the matrix. The REE are then processed over a HDEHP (di-2ethylhexyl-orthophosphoric acid)-coated Teflon powder column for the purification of Nd and Sm from the remaining matrix.

High precision ^{142}Nd was measured with a Thermo Scientific Triton Plus TIMS at the Laboratoire G-Time (ULB). Samples were measured as Nd metal on Re double filaments. Total measurements consisted of 18-54 blocks of 20 cycles, with an intensity on ^{142}Nd greater than 3V and rotating the amplifiers. Each measurement cycle consisted of a multi-static sequence across 3-lines (see Table S-2) following the method of Caro *et al.* (2006), Debaille *et al.* (2007) and Debaille *et al.* (2013) to ensure that differences in Faraday cup efficiency are cancelled and that all isobaric interferences could be monitored. Ratios are calculated for each line, which are subsequently corrected for mass fractionation via the exponential law, with all ratios corrected to ^{146}Nd/^{144}Nd of 0.7219. Cerium and Sm corrections are then applied, and final corrected ratios calculated for each individual line. The reported data is the average for each ratio across all three lines for each individual measurement (i.e. one round of all three lines being measured). This method also allows for the high precision measurement of ^{143}Nd. Isobaric interferences from Sm and Ce were minimal, with the largest Ce correction applied of 3 ppm. International reference material JNdi was run alongside the samples, with a reproducibility of μ^{142}Nd= 0.0 ± 2.0 during this analytical campaign (2σ, n=5).

Trace Elements

While the samples analysed in this work are the same as those from previous workers (Bau and Alexander, 2009; Viehmann *et al.,* 2014), the actual drilled samples are a separate aliquot, having been milled from the whole rock at separate times. As such, we performed trace element analyses when enough powder was left to ensure that there were no significant differences between the powder aliquots. Figure S-4 shows the chondrite normalised rare earth element data from this study (solid lines) and from Viehmann *et al.,* 2014 (dashed lines) for four samples. The measurements

are in good agreement except TM 3-5 showing the largest offset between the two studies, likely due to the resampling process. The remaining three samples are within the limits of inter-lab comparisons and uncertainty. Refer to Table S-3 for full trace element results.

$^{143}Nd/^{144}Nd$ Modelling

The ^{142}Nd and ^{143}Nd systematics are decoupled as they do not plot in the field defined by a two-stage model evolution (not shown). As such, the samples do not provide any hint on the timing of source model ages. In addition, Viehmann *et al.* (2014) already observed that the ^{143}Nd systematics is below the expected evolution of the depleted MORB mantle (DMM), ~+0.2 ± 1.7 ε-unit for the BIF in the present study (not considering TM 1-2 outlying at +10), compared to ~+4 for the DMM at 2.7 Ga, providing evidence that both volcanic and more felsic sources affected ancient Temagami seawater. Previous studies have shown decoupling of the $^{143\text{-}142}Nd$ systems, most notably in the Acasta Gneisses (Roth *et al.,* 2014), Nuvvuagittuq supracrustal belt (O'Neil *et al.,* 2008, 2012), Ameralik dykes (Rizo *et al.,* 2012) and the Schapenburg komatiite (Puchtel *et al.,* 2016). This decoupling can be attributed to a variety of factors, such as Sm/Nd fractionation after extinction of ^{146}Sm, or disturbance of the ^{147}Sm-^{143}Nd system. Therefore, it is not unusual for the $^{143\text{-}142}Nd$ systems to be decoupled in the Temagami BIF, which is also exacerbated by the likely multiple source components that are mixed into the seawater to provide the Nd compositions seen. While it is possible to have the ^{147}Sm-^{143}Nd system to be disturbed by later events, one should not assume that the ^{142}Nd systematic is always pristine. Indeed, we show here that the ^{142}Nd signature in the chert is likely a mixture between different continental sources with mantle hydrothermal-venting input. This is possibly the result of a changing activity and quiescence in the hydrothermal activity in the region surrounding the BIF deposition.

Supplementary Tables

Table S-1 **(over page)** Sm-Nd results for the Temagami BIF, and JNdi standards.

Sample	Lithology	Sm, ppm	Nd, ppm	ppm 142 Ce	142Nd/144Nd	2SD	143Nd/144Nd	2SD	145Nd/144Nd	2SD	146Nd/144Nd raw	148Nd/144Nd	2SD	150Nd/144Nd	2SD	147Sm/144Nd	u142Nd	2SD	143Nd/144Ndi	eNd
JNdi	standard	-	-	0.5	1.1418350	3E-06	0.512099	1E-06	0.348404	7E-07	0.722340	0.241579	1E-06	0.236449	2E-06	-	-	-	-	-
JNdi	standard	-	-	1.3	1.1418327	4E-06	0.512100	1E-06	0.348404	8E-07	0.722612	0.241580	1E-06	0.236449	2E-06	-	-	-	-	-
JNdi	standard	-	-	0.9	1.1418322	3E-06	0.512099	1E-06	0.348403	7E-07	0.721751	0.241578	9E-07	0.236448	2E-06	-	-	-	-	-
JNdi	standard	-	-	0.4	1.1418334	3E-06	0.512098	1E-06	0.348404	7E-07	0.721800	0.241580	1E-06	0.236448	2E-06	-	-	-	-	-
JNdi	standard	-	-	1.1	1.1418344	3E-06	0.512100	1E-06	0.348403	6E-07	0.722000	0.241579	1E-06	0.236447	2E-06	-	-	-	-	-
JNdi average				**0.8**	**1.1418335**	**2E-06**	**0.512099**	**1E-06**	**0.348404**	**9E-07**	**0.722101**	**0.241579**	**1E-06**	**0.236448**	**1E-06**					
TM 1-1	Fe-rich	0.79	4.33	0.9	1.1418417	3E-06	0.511053	1E-06	0.348404	9E-07	0.723021	0.241579	1E-06	0.236449	2E-06	0.1077	7.4	3.0	0.509134	0.0
TM 1-2	Chert	0.13	0.76	0.6	1.1418305	2E-06	0.511432	8E-07	0.348403	5E-07	0.722084	0.241577	7E-07	0.236444	1E-06	0.1003	-3.0	2.0	0.509646	10.0
TM 2-2	Chert	0.28	1.1	1.0	1.1418360	3E-06	0.511794	1E-06	0.348403	7E-07	0.722065	0.241578	1E-06	0.236444	2E-06	0.1481	1.9	2.6	0.509156	0.4
TM 2-3	Fe-rich	1.04	5.34	1.0	1.1418414	3E-06	0.511143	1E-06	0.348403	7E-07	0.722529	0.241578	1E-06	0.236449	2E-06	0.1151	7.1	2.6	0.509093	-0.8
TM 3-1	Chert	0.52	2.44	2.7	1.1418296	2E-06	0.511449	8E-07	0.348404	5E-07	0.720923	0.241576	8E-07	0.236440	1E-06	0.1264	-3.8	1.8	0.509198	1.2
TM 3-2	Fe-rich	1.19	6.16	2.2	1.1418408	3E-06	0.511181	1E-06	0.348403	8E-07	0.723009	0.241579	1E-06	0.236448	2E-06	0.1134	6.6	2.9	0.509160	0.5
TM 3-3*	Chert	0.13	0.6	1.9	1.1418329	6E-06	0.511473	2E-06	0.348404	1E-06	0.723505	0.241587	2E-06	0.236447	4E-06	0.1295	-0.9	5.1	0.509167	0.6
TM 3-4*	Fe-rich	0.82	4.07	3.2	1.1418354	5E-06	0.511198	2E-06	0.348403	1E-06	0.721464	0.241577	2E-06	0.236442	3E-06	0.1190	1.9	4.2	0.509079	-1.1
TM 3-5	Chert	0.11	0.56	0.5	1.1418297	3E-06	0.511287	1E-06	0.348403	7E-07	0.722124	0.241580	1E-06	0.236442	2E-06	0.1178	-3.7	2.9	0.509188	1.0
Chert weighted average																	**-2.5**	**3.8**		
Fe-rich weighted average																	**7.0**	**1.6**		

*not included in average calculations

Table S-2 Cup configuration of each line for ^{142}Nd TIMS measurement

Cup	L4	L3	L2	L1	Center	H1	H2	H3	H4
Line 1	^{140}Ce	^{142}Nd	^{143}Nd	^{144}Nd	^{145}Nd	^{146}Nd	^{147}Sm	^{148}Nd	^{150}Nd
Line 2		^{141}Pr	^{142}Nd	^{143}Nd	^{144}Nd	^{145}Nd	^{146}Nd	^{147}Sm	
Line 3		^{140}Ce	^{141}Pr	^{142}Nd	^{143}Nd	^{144}Nd	^{145}Nd	^{146}Nd	^{148}Nd

Table S-3 Trace element results for 4 of the samples analysed for ^{142}Nd along with analysis of reference material BHVO2 (Hawaiian Volcano Observatory Basalt).
Table S-3 is available for download (.xlsx) from the online version of this article at http://doi.org/10.7185/geochemlet.2421.

Supplementary Figures

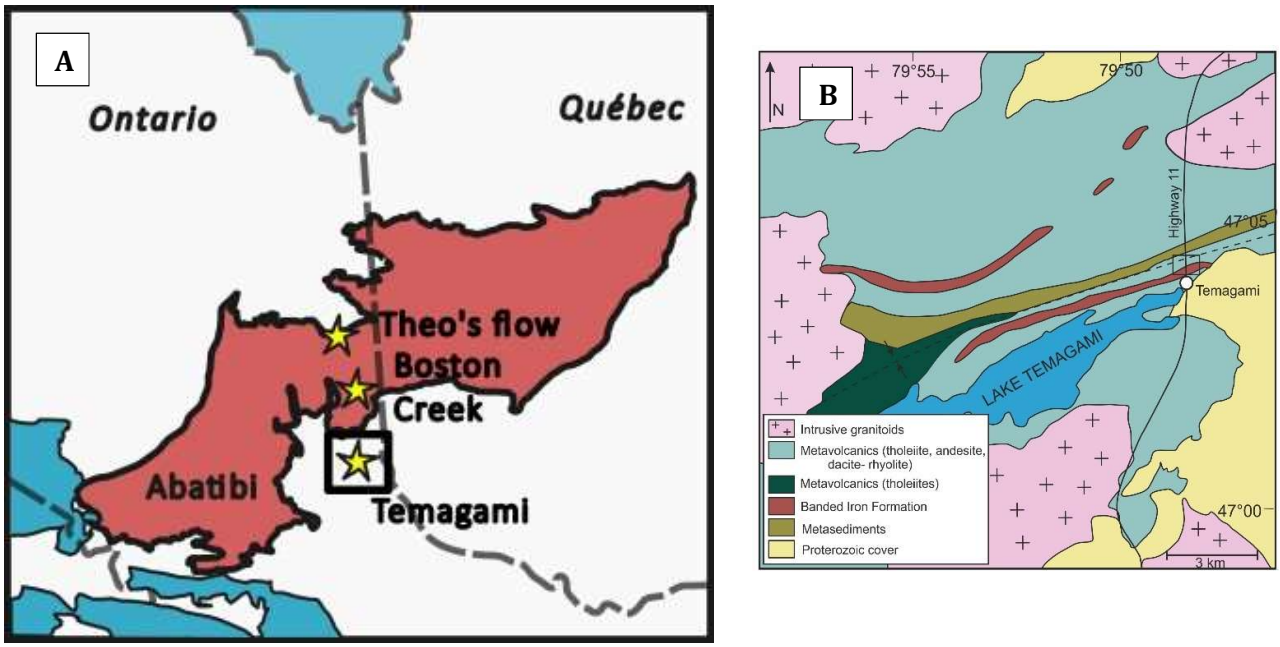

Figure S-1 **A)** Regional map of the Abibiti Greenstone belt in Canada, stars show locations of Theo's Flow (Debaille *et al.,* 2013), Boston Creek Komatiite (Puchtel *et al.,* 2018) and the Temagami. Square around Temagmi is region shown in panel b. **B)** Simplified geological map of the Temagami Greenstone Belt (modified from Bowins and Crocket, 1994; Bau *et al.,* 2022)

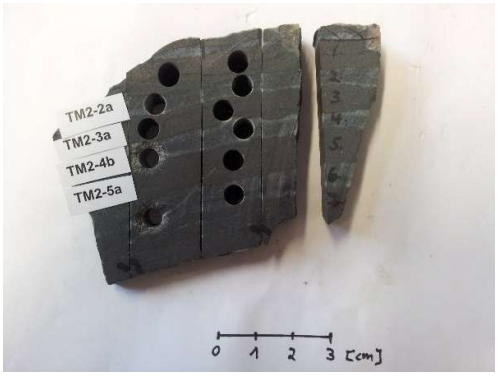

Figure S-2 Representative Temagami BIF sample with alternating chert and magnetite layers

Figure S-3 Photo of TM3 hand specimen, prior to sawing and milling for this study. As can be seen in the image, the hand samples shows small fractures and faults, which allows for the mixing of sample layers. During sampling it is possible that one of these areas was inadvertently sampled, leading to the similar ^{142}Nd compositions of TM3-3 and TM3-4.

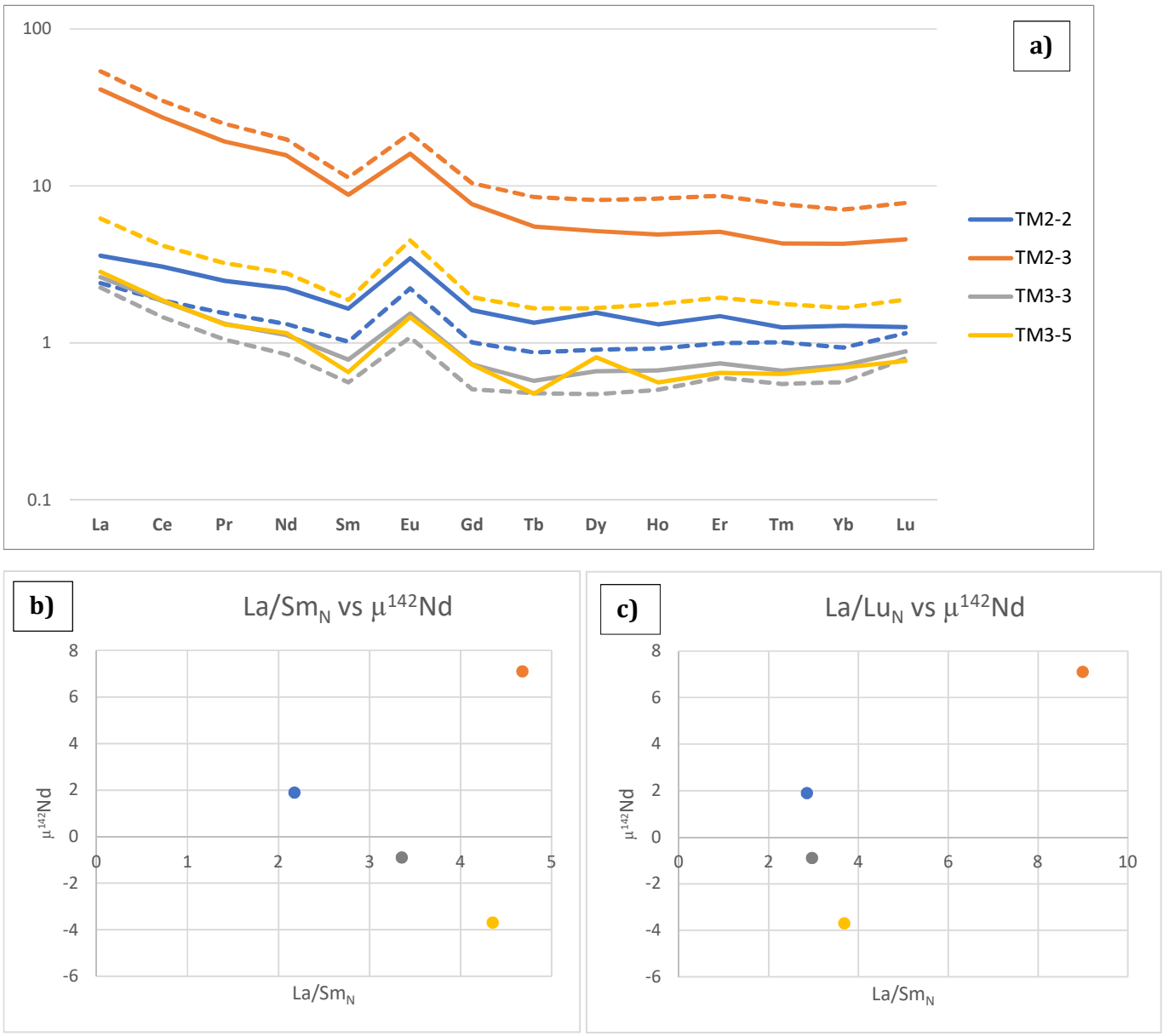

Figure S-4 **a)** Chondrite normalised rare earth element plots for four samples, comparing this study's results to previous work (Viehmann *et al.,* 2014), due to this study using re-sampled powders. The majority of samples are within analytical uncertainty and inter-lab comparisons expected for trace element results (± 10%). **b) and c)** La/Sm_N vs $\mu^{142}Nd$ and La/Lu_N vs $\mu^{142}Nd$ plots, for the same for samples as in a. Showing no correlation between trace elements and ^{142}Nd compositions.

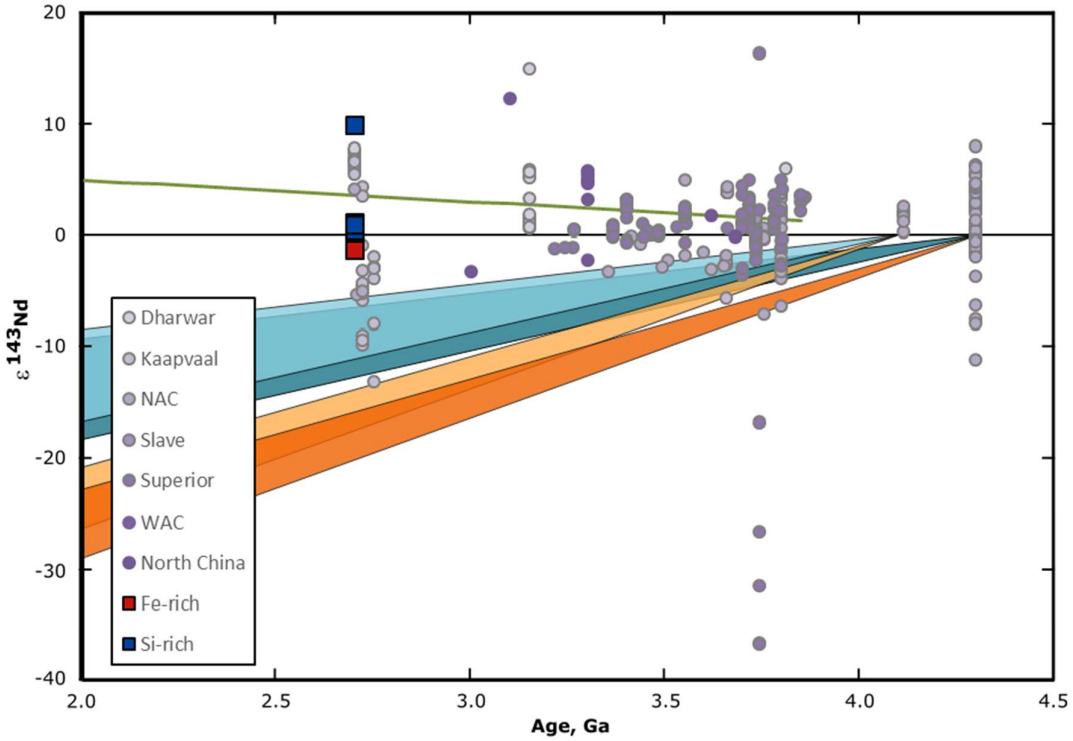

Figure S-5 Model showing the evolution of ε^{143}Nd through time, based on extraction of a TTG from a mafic (blue shaded areas) or felsic (orange shaded areas) source at 4.3 and 4.1 Ga. Model was calculated using a chondritic ^{147}Sm-^{143}Nd composition (from Bouvier *et al.,* 2008). Squares are data from this work, circles are the available ^{143}Nd literature data for samples that have also been analysed for ^{142}Nd. Dark green line is model from Debaille *et al.* (2013) showing trend of mixing in the mantle required to progress from the most positive ^{142}Nd values at 3.8 Ga to the +7 found in Abitibi at 2.7 Ga. (Caro *et al.,* 2003, 2017; Bennett *et al.,* 2007; O'Neil *et al.,* 2008, 2012, 2016; Rizo *et al.,* 2011, 2012; Debaille *et al.,* 2013; Puchtel *et al.,* 2013, 2016; Li *et al.,* 2017; Maya *et al.,* 2017; Morino *et al.,* 2017; Schneider *et al.,* 2018; O'Neil and Carlson, 2017; Wainwright *et al.,* 2019). Note that for the modelling (Fig. 2 and Fig. S-3.), we have used the approach of Morino *et al.* (2017) with bulk Earth (i.e. starting off point of the differentiation model) having a chondritic ^{143}Nd value but a terrestrial modern-like ^{142}Nd value.

Supplementary Information References

Bau, M., Alexander, B.W. (2009) Distribution of high field strength elements (Y, Zr, REE, Hf, Ta, Th, U) in adjacent magnetite and chert bands and in reference standards FeR-3 and FeR-4 from the Temagami iron-formation, Canada, and the redox level of the Neoarchean ocean. *Precambrian Research* 174, 337–346. https://doi.org/10.1016/j.precamres.2009.08.007

Bau, M., Frei, R., Garbe-Schönberg, D., Viehmann, S. (2022) High-resolution Ge-Si-Fe, Cr isotope and Th-U data for the Neoarchean Temagami BIF, Canada, suggest primary origin of BIF bands and oxidative terrestrial weathering 2.7 Ga ago. *Earth and Planetary Science Letters* 589, 117579. https://doi.org/10.1016/j.epsl.2022.117579

Bennett, V.C., Brandon, A.D., Nutman, A.P. (2007) Couple ^{142}Nd-^{143}Nd Isotopic Evidence for Hadean Mantle Dynamics. *Science* 318, 1907-1910. https://doi.org/10.1126/science.1145928

Bouvier, A., Vervoort, J.D., Patchett, P.J. (2008) The Lu-Hf and Sm-Nd isotopic composition of CHUR: Constraints from unequilibrated chondrites and implications for the bulk composition of terrestrial planets. *Earth and Planetary Science Letters* 273, 48-57. https://doi.org/10.1016/j.epsl.2008.06.010

Bowins, R.J., Heaman, L.M. (1991) Age and timing of igneous activity in the Temagami greenstone belt, Ontario: A preliminary report. *Canadian Journal of Earth Sciences* 28, 1873–1876. https://doi.org/10.1139/e91-167

Bowins, R.J., Crocket, J.H. (1994) Sulfur and carbon isotopes in Archean banded iron formations: Implications for sulfur sources. *Chemical Geology* 111, 307-323. https://doi.org/10.1016/0009-2541(94)90097-3

Caro, G., Bourdon, B., Birck, J-L., Moorbath, S. (2003) ^{146}Sm-^{142}Nd evidence from Isua metamorphosed sediments for early differentiation of the Earth's mantle. *Nature* 423, 428-432. https://doi.org/10.1038/nature01668

Caro, G., Bourdon, B., Birck, J-L., Moorbath, S. (2006) High-precision ^{142}Nd/^{144}Nd measurements in terrestrial rocks: Constraints on the early differentiation of the Earth's mantle. *Geochimica Cosmochimica Acta* 70, 164-191. https://doi.org/10.1016/j.gca.2005.08.015

Caro, G., Morino, P., Mojzsis, S. J., Cates, N. L., Bleeker, W. (2017) Sluggish Hadean geodynamics: Evidence from coupled ^{146,147}Sm–^{142,143}Nd systematics in Eoarchean supracrustal rocks of the Inukjuak domain (Québec). *Earth. And Planetary Science Letters* 457, 23-37. https://doi.org/10.1016/j.epsl.2016.09.051

Debaille, E., Brandon, A.D., Yin, Q.Z., Jacobsen, B. (2007) Coupled ^{142}Nd-^{143}Nd evidence for a protracted magma ocean in Mars. *Nature* 450, 525-528. https://doi.org/10.1038/nature06317

Debaille, V., O'Neil, C., Brandon, A. D., Haenecour, P., Yin, Q-Z., Mattielli, N., Treiman, A.H. (2013) Stagnant-lid tectonics in early Earth revealed by ^{142}Nd variations in late Archean rocks. *Earth Planetary Science Letters* 373, 83-92. https://doi.org/10.1016/j.epsl.2013.04.016

Fyon, J.A., Cole, S. (1989) Geology of part of the Temagami greenstone belt, District of Nipissing, including relationships between lithological, alteration, and structural features and precious-metal occurrences. In: *Summary of field work and other activities 1989*, Ontario Geological Survey Miscellaneous Paper 146, 108–115.

Li, C.-F., Wang, X.-C., Wilde, S.A., Li, X.-H., Wang, Y.-F., Li, Z. (2017) Differentiation of the early silicate Earth as recorded by ^{142}Nd-^{143}Nd in 3.8–3.0 Ga rocks from the Anshan Complex, North China Craton. *Precambrian Research* 301, 86-101. https://doi.org/10.1016/j.precamres.2017.09.001

Li, C.-F., Wang, X.-C., Li, Y.-L., Chu, Z.-Y., Guo, J.-H., Li, X.-H. (2015) Ce-Nd separation by solid-phase micro-extraction and its application to high-precision ^{142}Nd/^{144}Nd measurements using TIMS in geological materials. *Journal of Analytical Atomic Spectrometry* 30, 895-902. https://doi.org/10.1039/C4JA00328D

Maya, J.M., Bhutani, R., Balakrishnan, S., Sandhya, S.R. (2017) Petrogenesis of 3.15 Ga old Banasandra komatiites from the Dharwar craton, India: Implications for early mantle heterogeneity. *Geoscience Frontiers* 8, 467-481. https://doi.org/10.1016/j.gsf.2016.03.007

Morino, P., Caro, G., Reisburg,L., Schumacher, A. (2017) Chemical stratification in the post-magma ocean Earth inferred from coupled ^{146,147}Sm–^{142,143}Nd systematics in ultramafic rocks of the Saglek block (3.25–3.9 Ga; northern Labrador, Canada). *Earth Planetary Science Letters* 463, 136-150. https://doi.org/10.1016/j.epsl.2017.01.044

Mundl-Petermeier, A., Viehmann, S., Tusch, J., Bau, M., Kurzweil, F., Münker, C. (2022) Earth's geodynamic evolution constrained by 182W in Archean seawater. *Nature Communications* 13, 2701. https://doi.org/10.1038/s41467-022-30423-3

O'Neil, J., Carlson R.W. (2017) Building Archean cratons from Hadean mafic crust. *Science* 355, 1199-1202. https://doi.org/10.1126/science.aah3823

O'Neil, J., Carlson, R.W., Franics, D., Stevenson, R.K. (2008) Neodymium-142 Evidence for Hadean Mafic Crust. *Science* 321, 1828-1831. https://doi.org/10.1126/science.1161925

O'Neil, J., Carlson, R.W., Paquette, J-L., Francis, D. (2012) Formation age and metamorphic history of the Nuvvuagittuq Greenstone Belt. *Precambrian Res*earch 220-221, 23-44. https://doi.org/10.1016/j.precamres.2012.07.009

O'Neil, J., Rizo, H., Boyet, M., Carlson, R.W., Rosing, M.T. (2016) Geochemistry and Nd isotopic characteristics of Earth's Hadean mantle and primitive crust. *Earth Planetary Science Lett*ers 442, 194-205. https://doi.org/10.1016/j.epsl.2016.02.055

Puchtel, I.S., Blichert-Toft, J., Touboul, M., Walker, R.J., Byerly, G.R., Nisbet, E.G., Anhaeusser, C.R. (2013) Insights into early Earth from Barberton komatiites: Evidence from lithophile isotope and trace element systematics. *Geochimica. Cosmochimica Acta* 108, 63-90. https://doi.org/10.1016/j.gca.2013.01.016

Puchtel, I.S., Blichert-Toft, J., Touboul, M., Horan, M.F., Walker, R.J. (2016) The coupled ^{182}W-^{142}Nd record of early terrestrial mantle differentiation. *Geochemistry Geophysics Geosys*tems 17, 2168-2193. https://doi.org/10.1002/2016GC006324

Puchtel, I.S., Blichert-Toft, J., Touboul, M., Walker, R.J. (2018) 182W and HSE constraints from 2.7 Ga komatiites on the heterogeneous nature of the Archean mantle. *Geochimica et Cosmochimica Acta* 228, 1-26. https://doi.org/10.1016/j.gca.2018.02.030

Rizo, H., Boyet, M., Blichert-Toft, J., Rosing, M. (2011) Combined Nd and Hf isotope evidence for deep-seated source of Isua lavas. *Earth Planetary Science Letters* 312, 267-279. https://doi.org/10.1016/j.epsl.2011.10.014

Rizo, H., Boyet, M., Blichert-Toft, J., O'Niel, J., Rosing M. T., Paquette, J-L. (2012) The elusive Hadean enriched reservoir revealed by142Nd deficits in Isua Archaean rocks. *Nature* 491, 96-100. https://doi.org/10.1038/nature11565

Roth, A.S.G., Bourdon, B., Mojzsis, S.J., Rudge, J.F., Guitreau, M., Blichert‐Toft, J. (2014) Combined ^{147,146}Sm-^{143,142}Nd constraints on the longevity and residence time of early terrestrial crust. *Geochemistry, Geophysics, Geosystems* 15, 2329–2345. https://doi.org/10.1002/2014GC005313

Saji, N.S., Wielandt, D., Paton, C., Bizzarro, M. (2016) Ultra-high-precision Nd-isotope measurements of geological materials by MC-ICPMS. *Journal Analytical Atomic Spectrom*etry 31, 1490-1504. https://doi.org/10.1039/C6JA00064A

Schneider, K.P., Hoffman, J.E., Boyet, M., Münker, C., Kröner, A. (2018) Coexistence of enriched and modern-like ^{142}Nd signatures in Archean igneous rocks of the eastern Kaapvaal Craton, southern Africa. *Earth Planetary Science Letters* 487, 54-66. https://doi.org/10.1016/j.epsl.2018.01.022

Viehmann, S., Hoffmann, J.E., Münker, C., Bau, M. (2014) Decoupled Hf-Nd isotopes in Neoarchean seawater reveal weathering of emerged continents. *Geology* 42, 115–118. https://doi.org/10.1130/G35014.1

Wainwright, A.N., El Atrassi, F., Debaille, V., Mattielli, N. (2019) Geochemistry and petrogenesis of Archean mafic rocks from the Amsaga area, West African craton, Mauritania. *Precambrian Research 324*, 208-219. https://doi.org/10.1016/j.precamres.2019.02.005